JOURNAL OF MATERIALS SCIENCE 39 (2004) 6743–6755

Advanced physical characterisation of the structural evolution of amorphous $(TiO_2)_x(SiO_2)_{1-x}$ sol-gel materials

G. W. WALLIDGE
Department of Physics, University of Warwick, Coventry, CV4 7AL, UK

R. ANDERSON, G. MOUNTJOY, D. M. PICKUP
School of Physical Sciences, University of Kent, Canterbury, Kent, CT2 7NR, UK

P. GUNAWIDJAJA
Department of Physics, University of Warwick, Coventry, CV4 7AL, UK

R. J. NEWPORT
School of Physical Sciences, University of Kent, Canterbury, Kent, CT2 7NR, UK

M. E. SMITH*
Department of Physics, University of Warwick, Coventry, CV4 7AL, UK
E-mail: m.e.smith.1@warwick.ac.uk

Amorphous $(TiO_2)_x(SiO_2)_{1-x}$ ($x = 0.08$, 0.18, and 0.41) sol-gel formed materials have been characterised by a combination of X-ray and neutron diffraction, infra-red and ^{29}Si and ^{17}O magic angle spinning NMR spectroscopy. This combination allows new insight into the fundamental structural role titanium additions play in silica, entering the network at $x = 0.08$ but largely phase separating at $x = 0.41$. At an intermediate value of $x = 0.18$ there is complex coordination behaviour with initially some Ti–O–Ti linkages forming and both TiO_4 and TiO_6 coordinations present. It appears that at 500°C for the $x = 0.18$ sample all titanium is present in Ti–O–Si linkages but that this situation is unstable on further calcination. The new information presented here is amalgamated with that from our previous EXAFS, XANES and SAXS on the same samples to produce the most complete view to date of the local and mesoscopic structural behaviour of the $(TiO_2)_x(SiO_2)_{1-x}$ system produced by the sol-gel method.

1. Introduction

1.1. General background to characterisation methodology

One of the most challenging contemporary problems for structural materials science is to collect sufficiently comprehensive experimental data sets from complementary probe techniques to be able to describe accurately and unambiguously the structure of amorphous materials and follow how their structure changes with processing. To better understand these complex problems demands the use of a range of modern advanced characterisation methods. A range of techniques that probe different length scales is shown in Fig. 1, with the subset of those used to probe the TiO_2-SiO_2 sol-gel materials in this study indicated. The standard bulk characterisation techniques such as thermal analysis and mass loss provide background information about change as a material's structure evolves during processing. For amorphous materials diffraction techniques provide much information via a pairwise (i.e., atom-atom) correlation function $T(r)$ when carried out with intense, modern X-ray and neutron sources. The individual correlations are be disentangled by comparing X-ray (XRD) and neutron diffraction (ND) through the contrast provided by variations in the relative scattering of the different elements between the two techniques. The diffraction patterns provide information about the short- and medium-range structure (i.e., bond lengths, bond angles and coordination numbers) of a material. With amorphous materials it is important that the possibilities of phase separation and inhomogeneity are excluded as sources of the structural features that are seen in the short- and medium-range structure. The presence of regions of different composition and their physical disposition with respect to each other—the mesoscopic inhomogeneity, can be revealed by electron microscopy and energy dispersive X-ray spectroscopy (EDS). An alternative approach for determining mesoscopic homogeneity is to use small angle X-ray (SAXS) and neutron (SANS) scattering.

*Author to whom all correspondence should be addressed.

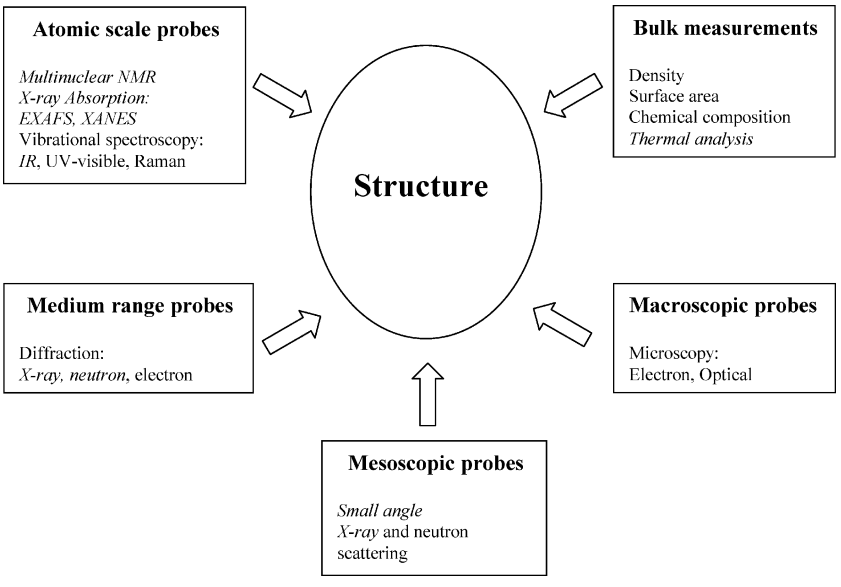

Figure 1 Schematic view of a characterisation methodology available for complex amorphous materials, with the techniques used on the samples presented in this paper shown in italics.

Vibrational techniques (e.g., IR, Raman) provide information about the types of bonds present which are affected by short, and to some extent the medium-range structure. Extended X-ray absorption fine structure (EXAFS) provides accurate bond length information, and hence insight into coordination, and X-ray absorption near edge structure (XANES) can be used to fingerprint coordination. Nuclear magnetic resonance (NMR) has probably the shortest length scale of all the techniques used here. NMR is element specific with the most direct information available from the resonance position which is largely determined by the chemical shift. The chemical shift is determined by the bonding environment of the nucleus which is affected by factors such as the connectivity. To get the most complete picture of the structure from NMR it is best to obtain information from as many of the different nuclear perspectives as possible.

1.2. TiO_2-SiO_2 sol-gels materials and previous characterisation

Mixed titania:silica sol-gels ($(TiO_2)_x(SiO_2)_{1-x}$) exemplify the generic challenge to the characterisation of amorphous materials. Silica containing a few mol% titania forms ultralow thermal expansion glasses [1] and catalysts and catalytic support media [2]. Sol-gel prepared TiO_2-SiO_2 is used in a number of optical applications, such as coatings with tailored refractive indices [3] and as wave guides [4]. The properties of amorphous titania:silica materials depend on their composition, homogeneity and structure. The atomic scale structural homogeneity in particular has a strong influence. The importance of the catalytic properties of these materials is emphasised by the extensive characterisation studies that have been carried out to understand the relationship between structure and properties and was reviewed recently by Davis and Lui [5].

The sol-gel synthesis method [1] involves the hydrolysis and condensation of metal alkoxides at low temperature, which allows a high level of atomic mixing and (potentially) high porosity. In the preparation of $(TiO_2)_x(SiO_2)_{1-x}$, the more rapid rate of reaction of the titanium precursors can lead to phase separation, due to the formation of Ti-rich regions. Phase separation has a considerable effect on the attributes of the material and is particularly detrimental to catalysis reactions involving hydrogen peroxide (H_2O_2) [2]. To optimise homogeneity the silicon-bearing precursor is partially hydrolysed before the addition of the titanium alkoxide using the method of Yoldas [6]. This encourages the formation of Ti–O–Si linkages, which allows for a larger proportion of titanium to be incorporated in the silica sol-gel before the onset of phase separation.

Previous work using ^{17}O and ^{29}Si MAS NMR [7] and diffraction techniques [8] on unheated $(TiO_2)_x(SiO_2)_{1-x}$ xerogels with $x = 0.08$, 0.18, and 0.41 formed the starting point for this current study, wherein diffraction (both X-ray and neutron), NMR and FTIR data has been collected for unheated samples and after calcination at a number of temperatures (250, 500, 750, and 850°C). The three compositions were carefully chosen to represent regions of distinct structural behaviour in this system. At $x = 0.08$ the material is well inside the solubility limit for titanium in silica glasses, whereas at $x = 0.41$ it is well into the two phase titania/silica region. Samples with $x = 0.18$ are close to the boundary between these behaviours. This composition is beyond the solubility limit for titanium in conventional melt-quenched titania-silica glasses. However it is possible to produce an initially single phase xerogel at this composition, which phase separates with heat treatment. Thus the structure of $x = 0.18$ xerogels is complex and of particular interest. These $(TiO_2)_x(SiO_2)_{1-x}$ samples are henceforth designated SiTi-8, SiTi-18 and SiTi-41.

^{29}Si MAS NMR is a well developed technique for examining the silicon environment, providing information about the connectivity of silicon, where Q^n represents a $Si(OM)_n(OT)_{4-n}$ terahedron, and M denotes

a tetrahedral framework titanium or silicon, T a terminating hydroxyl or ethoxy group, or maybe a negative charge for a non-bridging oxygen [9, 10]. ^{17}O NMR is a much less well developed approach than ^{29}Si, since its natural abundance (0.037%) usually demands isotopic enrichment, but it can in principle provide knowledge about the different oxygen sites that are present, e.g., Ti—O—Ti, Ti—O—Si, Si—O—Si, giving unique and direct information about the atomic scale distribution of oxygen sites [10]. In the diffraction studies XRD is insensitive to hydrogen, but relatively sensitive to titanium ($Z = 22$) compared to the next heaviest element, Si ($Z = 14$). ND gives roughly equal weighting to all elements. The high sensitivity of FTIR to groups containing hydrogen (e.g., —OH and —CH) makes this technique particularly useful when examining the organic and hydroxyl content of these xerogels. Despite the extensive study of Ti—Si materials much of the structural data remains ambiguous. This study has collected a comprehensive set of experimental data that allows models of the structural development of these materials to be rigorously tested.

2. Experimental

2.1. Sample preparation and thermal analysis

The samples were prepared using the precursors tetraethyl orthosilicate (TEOS, Aldrich 98%) and titanium (IV) isopropoxide (Ti (OPr^i)$_4$, Aldrich 97%). Propan-2-ol (IPA, BDH 99%) was used as a mutual solvent, and concentrated HCl as a catalyst. All reagents were handled in a dry box under dry nitrogen with subsequent transfer being done either in sealed containers or syringes.

All samples were prepared using the method of Yoldas [6], using prehydrolysis of the TEOS followed by addition of the Ti(OPr^i)$_4$ and the remaining water. Samples for ^{17}O NMR were prepared using 10 mol% ^{17}O-enriched water for the hydrolysis. For the SiTi-8 and -18 samples TEOS was prehydrolysed in the molar ratio 1:1:1 TEOS:water:IPA for two hours at pH = 1 before the appropriate amounts of Ti(OPr^i)$_4$ and water were added to give a ratio of (Ti + Si):H_2O of 1:2. The mixtures were then stirred continuously until they gelled. This method was not optimal for the SiTi-41 gels so that an alternative pre-hydrolysis regime was used with a molar ratio 2:6:2:1 TEOS:H_2O:IPA:HCl. After prehydrolysis for three hours Ti(OPr^i)$_4$ and water were then added as before. It should be noted that much of the water in the above ratio for the prehydrolysis resulted from the HCl used.

To promote cross-linking all samples were allowed to age for 2 weeks after gelation, in sealed containers to prevent drying. The samples were then dried for 2 days in air, ground to a fine powder and dried under vacuum until no further weight loss was observed. The samples were divided into separate portions, which were then calcined to the required temperatures in air, using a vertical tube furnace. A heating rate of 5°C/min was used and the final temperature held for two hours. The furnace was then allowed to cool at a maximum rate of 5°C/min. The ^{17}O-labelled samples were heated in a horizontal tube furnace under a nitrogen atmosphere. The heating regime was similar to that used for other samples, except that the cooling rate was much lower (∼1°C/min). The samples were not withdrawn until the furnace had cooled to ∼40°C. The differences were to prevent the exchange of ^{17}O with ^{16}O, from the atmosphere, which can occur at elevated temperatures. Our studies have compared the effects of the different heating regimes on the structure. It appears that equilibrium is rapidly achieved at temperature, so that heating directly to a given temperature or stepping through various temperatures on the way to the same target temperature have no discernable effect on the structure [11]. Also it was shown that air and nitrogen have effectively no difference on the evolution of the structure except that the residual organics are removed at a slightly lower temperature under air [11].

With sol-gel prepared samples there is always the question of the reproducibility of the "structure". On the TiO_2-SiO_2 system we have not only analysed the same sample several times but also made up the same composition independently on a number of occasions as well. When the same preparation procedure is followed as here, using ^{29}Si MAS NMR data as a guide, reproducibility of the structure as indicated by the Q speciation is well within the quoted errors.

Thermogravimetric analysis was carried out using a Stanton Redcroft TG 750/770 apparatus. The samples were heated under a flow of air at a heating rate of 2°C/min up to ∼1000°C.

2.2. FTIR

The infrared spectra were collected using conventional transmission geometry with a Biorad FTS175C spectrometer controlled by Win-IR software. Samples were diluted using dry KBr, pressed into pellets and scanned in the range 4000–400 cm^{-1}, with a resolution of 4 cm^{-1}. The spectrum of a blank KBr pellet was also measured to allow background subtraction.

2.3. MAS NMR

^{29}Si NMR data were collected using magic angle spinning (MAS) on a Bruker MSL 300 spectrometer equipped with an Oxford Instruments 7.05 T magnet. Some additional ^{29}Si MAS NMR data was collected on a Chemagnetics CMX Infinity 360 spectrometer with an Oxford Instruments 8.45 T magnet. These instruments were run at frequencies of 59.9 and 71.54 MHz respectively using a Bruker 7 mm MAS probe and spinning speeds of 2.5–4 kHz. A recycle delay of 15–30 s was used to avoid saturation of the magnetisation. Tetramethylsilane (TMS) was used as an external reference compound at 0 ppm.

^{17}O NMR data were collected using MAS on Chemagnetics CMX Infinity spectrometers equipped with 14.1 T and 5.6 T magnets, and a Bruker MSL 360 equipped with an 8.45 T magnet at resonance frequencies of 81.342, 32.27 and 48.82 MHz respectively. 4 mm MAS NMR probes were used, spinning at speeds

of 10–12.5 kHz with recycle delays of 1–2 s which were sufficient to avoid saturation effects. Tap water was used as an external reference compound at 0 ppm.

2.4. Diffraction

X-ray diffraction data were collected in transmission mode using Debye-Scherrer geometry at a wavelength 0.485 Å on Station 9.1 at the SRS, Daresbury Laboratory, UK. The samples were mounted as fine powders in an aluminium annulus of thickness 0.5 mm, with kapton foil windows. In addition, the diffraction pattern for an empty cell was collected for the purpose of background subtraction. Useful data was collected for 2θ in the range 1.8° to 125°, giving a Q_{max} of 23 Å^{-1}.

The data were corrected for dead time, variation in X-ray beam intensity, polarisation, absorption, background and path length variations [12]. Coherent form factors were calculated according to Cromer and Mann [13], and incoherent scattering intensities according to Hajdu [14]. All other coefficients were taken from the International Tables for Crystallography [15].

Neutron diffraction data were collected using the Small Angle Neutron Diffractometer for Amorphous and Liquid Samples (SANDALS) [16] at the ISIS neutron spallation source of the Rutherford Appleton Laboratory, UK. This instrument gives continuous angular coverage between $2\theta = 3.8°$ and 39° using neutrons with wavelengths between 0.01 and 4.5 Å giving a Q_{max} of 50 Å^{-1}. The use of high energy (short λ) neutrons at low values of 2θ helps to minimise experimental difficulties due to inelastic and incoherent scattering from hydrogen which is a significant problem in the initial and low temperature gels. The samples were fine powders and were placed in 6 mm diameter cylindrical vanadium cans. In addition to the samples diffraction patterns were collected for the empty diffractometer, an empty can for background subtraction, and a vanadium rod for normalisation.

Neutron diffraction data was analysed using the Atlas suite of programs [17], as outlined by Hannon *et al.* [18]. The samples that were examined contained significant amounts of hydrogen (up to 35 at% at the lower temperatures). This gives rise to a significant level of incoherent scattering so that Chebyshev polynomials were fitted to correct for this. The attainable Q_{max} was progressively reduced with increasing hydrogen content (e.g., from 40 Å^{-1} for $x = 0.18$ calcined to 750°C, to 34.6 Å^{-1} for $x = 0.18$ calcined to 250°C).

Both XRD and ND are governed by the same physical principles. After data reduction $S(Q)$ data is obtained which is related to the real space pair correlation function, $T(r)$, by Fourier transformation (FT) [18]. $S(Q)$ is defined as,

$$S(Q) = 1 + \frac{1}{Q}\int_0^\infty (T(r) - T^0(r))\sin(Qr)\mathrm{d}r \quad (1)$$

where Q is

$$Q = \frac{4\pi}{\lambda}\sin(\theta). \quad (2)$$

2θ is the scattering angle and λ is the wavelength of the diffracted radiation. From Equation 1 it can be shown that,

$$T(r) = \frac{2}{\pi}\int_0^\infty QS(Q)\sin(Qr)\mathrm{d}r + T^0(r). \quad (3)$$

For multicomponent systems, such as under discussion here, $T(r)$ can also be defined in terms of $T_{ij}(r)$ the partial correlation functions for pairs of atomic species i and j as

$$T(r) = \sum_{i,j} n_i n_j Z_i Z_j T_{ij}(r) \quad (4)$$

and $T^0(r)$ is defined as,

$$T^0(r) = 4\pi r\rho\left(\sum_i n_i Z_i\right)^2, \quad (5)$$

where ρ is the atomic number density, n_i is the fraction of, and Z_i is the atomic number (X-rays) or coherent scattering length (b_i) (neutrons), for atom type i. It is possible to obtain structural information from $T(r)$ (e.g., bond lengths, coordination numbers etc.) via a modelling process.

Fitting Gaussians directly to $T(r)$ is problematic, due to truncation effects in the FT since the upper limit for integration in Equation 1 is typically ~20–50 Å^{-1} [19]. Truncation effects can be reduced by the use of a window function, however this is at the expense of peak shape and width. These problems can be largely overcome by fitting to a model $S(Q)$ with peaks in $T(r)$. The model $S(Q)$ is generated and transformed using the same Q range and window function as the data, it is then refined by iteration [20]. It is necessary to include all the major peaks in $T(r)$ to produce reliable results, even if these features do not yield useful structural information (in this work all features up to 3.1 Å were fitted).

The effective resolution of features within $T(r)$ is,

$$\Delta r \sim \frac{2\pi}{Q_{max}}. \quad (6)$$

3. Results

3.1. Thermal analysis

The fractional change of mass of the three samples on heating to 800–1000°C is shown in Fig. 2. The three major causes of mass loss in these samples with increasing temperature are removal of (i) physisorbed molecules such as water and alcohols, (ii) residual organic alkoxide fragements and (iii) structural hydroxyls. The initial steep loss of mass is associated with the physisorbed molecules and it appears that the SiTi-8 sample has

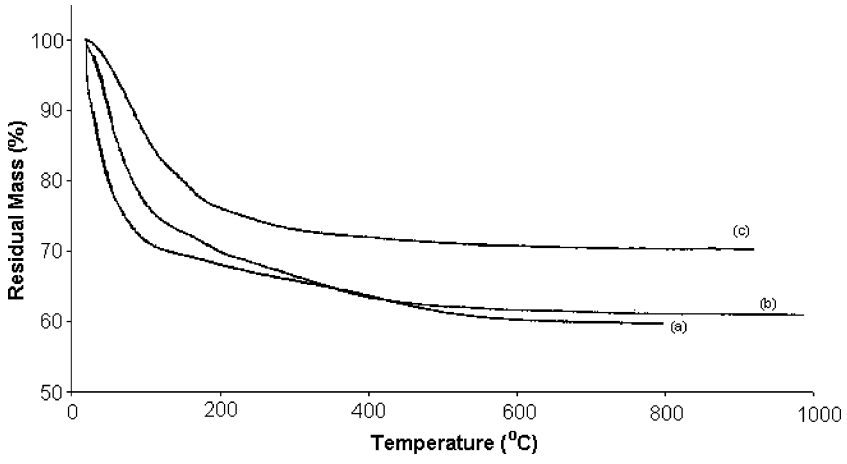

Figure 2 TGA traces of the SiTi-8 (a), SiTi-18 (b) and SiTi-41 (c) samples.

more of this (as a fraction of its total mass). Then between 150 and 250°C there is a change of slope and further mass loss. Our ^{13}C NMR study [11] of these systems has shown that the initial gels contain significant organic fragments remaining from the alkoxide precursor. These fragments are nearly all removed during this stage. The final much more gradual loss of mass in all these sample is the removal of protons from the structure that are lost as water. These protons are mostly present as structural hydroxyls groups which have previously been quantified by ^{1}H NMR [11]. The loss of hydroxyls results in further cross-linking of the silicate network, increasing the amount of Q^4 species in the network (see below). ^{1}H NMR work has shown that by 750°C there is still a measurable but very weak proton signal ascribed to a small residual amount of surface adsorbed protons rather than from structural hydroxyls. By this temperature the mass of all 3 samples has stabilised with the total mass losses of SiTi-8, -18, and -41 being 41, 39 and 30% respectively.

3.2. FT-IR

The FT-IR data is displayed in Fig. 3, and the main features and their assignments are listed in Table I. The broad feature at 3500 cm^{-1} is assigned to O─H stretching (ν_1(OH) at 3500 cm^{-1} and ν(H$_2$O) at 3300 cm^{-1}) [21]. The band at 1650 cm^{-1} is assigned to H─O─H bending vibrations (ν_2(H$_2$O)). The peaks at 1190, 1080, and 790 cm^{-1} are characteristic of the silica network (ν_{as}(SiO$_4$) LO, ν_{as}(SiO$_4$) TO and ν_s(SiO$_4$) respectively). Finally, the feature at 950 cm^{-1} can be assigned to two overlapping peaks ν(Si─O─H) and ν(Ti─O─Si) [22].

3.3. NMR

The ^{29}Si MAS NMR data were analysed by applying an exponential weighting function to the free induction decay prior to FT to remove high frequency noise producing 40 Hz line broadening which is small compared to the intrinsic linewidths. Three separate

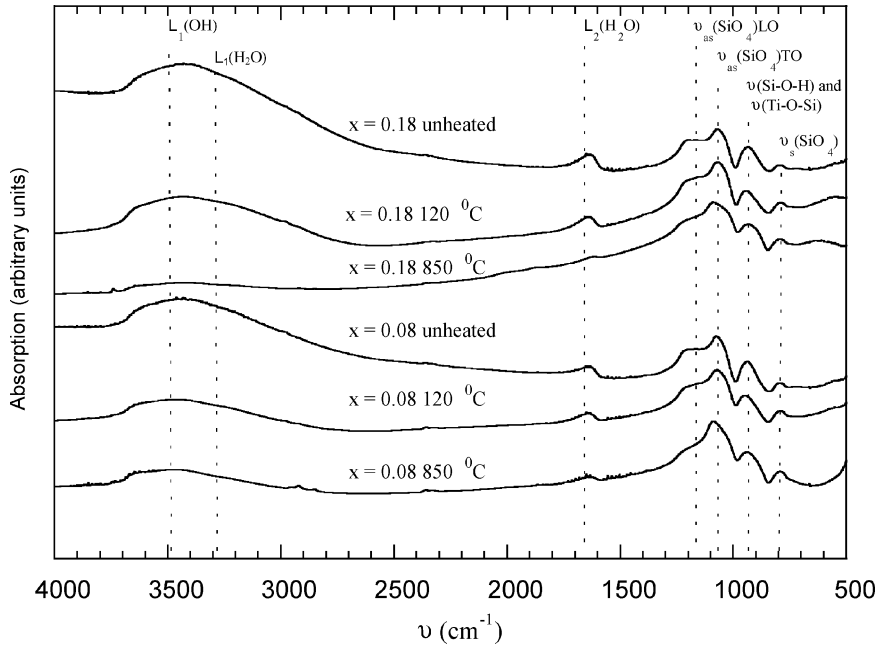

Figure 3 FT-IR data for SiTi-8 and -18 samples after various heat treatments.

TABLE I Summary of FT-IR data for $(TiO_2)_x(SiO_2)_{1-x}$ samples with varying calcinations temperature and composition

Sample (x, calcination temperature)	ν_1 (H_2O) (cm^{-1})	ν (OH) (cm^{-1})	ν_2 (H_2O) (cm^{-1})	ν_{as} (SiO_4) LO (cm^{-1})	ν_{as} (SiO_4) TO (cm^{-1})	ν (Si—OH), ν (Si—O—Ti) (cm^{-1})	ν_5 (SiO_4) (cm^{-1})
0.08, NHT	3454 vs, vb		1640 m	1179 sh	1080 s, b	942 s, b	798 w
0.08, 120°C	3466 s, vb	3255 sh	1647 m	1179 sh	1077 s, b	952 m, b	796 m
0.08, 850°C	3467 m, vb	3263 sh	1644 w	1205 sh	1094 s, b	942 m, b	798 m
0.18, NHT	3447 vs, vb		1644 m	1172 sh	1078 s, b	941 s, b	798 w
0.18, 120°C	3440 s, vb	3229 sh	1645 m	1182 sh	1076 s, b	947 s, b	794 m
0.18, 850°C	3427 m, vb	3232 sh	1624 w	1200 sh	1096 s, b	938 m, b	797 m

NHT—unheated gel.
vs, s, m, w correspond to very strong, strong, medium and weak respectively. vb, b and sh correspond to very broad, broad, and shoulder respectively.

peaks were detected at −94, −100, and −110 ppm and can be assigned to Q^2, Q^3 and Q^4 respectively [11, 23]. The spectra were simulated by fitting three Gaussians, one for each Q-species. Gaussians are reasonable approximations to the ^{29}Si MAS NMR lineshapes in such glassy materials where the linewidths are largely determined by chemical shift dispersion. The spectra and simulations for the SiTi-8 sample unheated and calcined at 750°C are shown in Fig. 4. The simulation results for all samples are summarised in Table II. It can be seen that in all the initial gels there are significant amounts of Q^2 and Q^3 as well as some Q^4. As the samples are heated there is a reduction in the amounts of Q^2 and Q^3 relative to Q^4 which results in the average Q speciation increasing as shown in Fig. 4c. In the initial gels there is some variation in the Q speciation which must indicate different retention of hydroxyls and/or alkoxy groups. However after heating to 750°C the average Q speciation has become very similar with the fraction of Q^4 ∼90%. As the samples are heated SiTi-8 and -0.18 show a progressive increase in the average Q speciation, whereas that for the SiTi-41 sample it remains approximately constant at ≤500°C, followed by a rapid increase in the amount of Q^4 at higher temperatures.

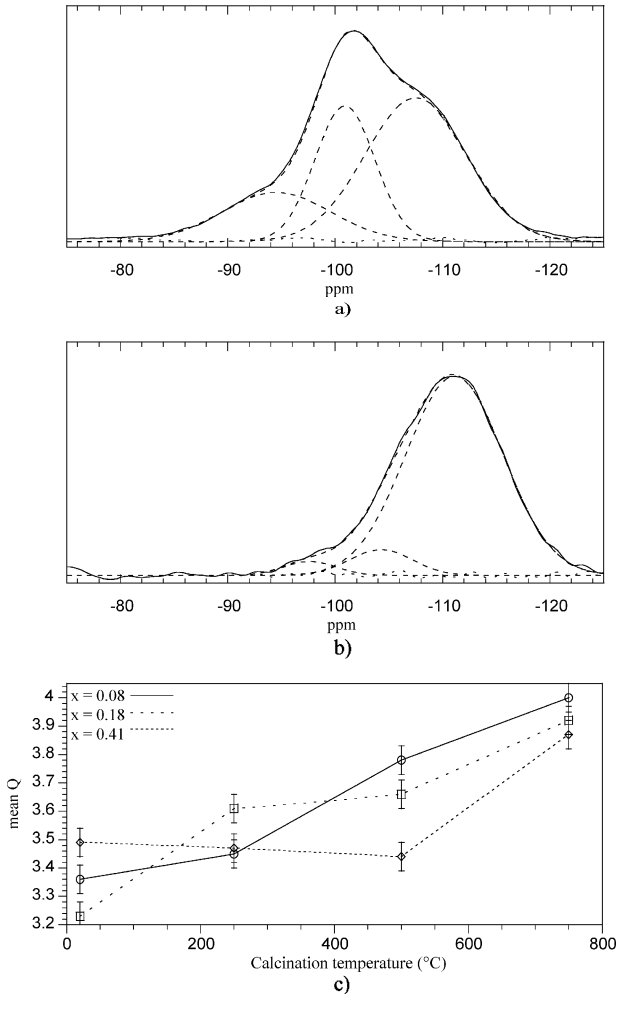

Figure 4 ^{29}Si MAS NMR data together with simulations of SiTi-18 (a) unheated and (b) heated to 750°C, (Solid line is the experimental data, and the individual Gaussians, total fit and residual are shown as dashed lines), and (c) the variation in the average Q^n speciation with heat treatment.

The ^{17}O MAS NMR spectra collected at 5.6 T are shown in Fig. 5 for all these samples. Most of the ^{17}O MAS NMR spectra are dominated by a feature extending below 0 ppm and centred at ∼−100 ppm, which is largely due to the second-order quadrupolar lineshape from Si—O—Si units [7, 10] with some contribution from Si—OH [10, 24, 25]. The broad resonances peaking at ∼235 ppm can be assigned to Ti—O—Si linkages [7, 10, 26–28] although some contribution from Ti—OH may also occur in this region [29, 30]. There is also some intensity above the baseline between 235 ppm and the Si—O—Si resonance, although it is not a distinct, separate peak. For the SiTi-18 sample heated to 250°C a shoulder at 110 ppm can be seen (indicated by an arrow in the figure). Additional resonances can be observed at 750, 530, and 360 ppm in some spectra which correspond to Ti—O—Ti linkages in OTi_2 $OTi_3$and OTi_4 respectively [7, 10, 30, 31]. Other minor features in these spectra are spinning sidebands as marked.

The magnetic field variation of these ^{17}O MAS NMR spectra is extremely revealing and is shown for the SiTi-18 sample in Fig. 6 for magnetic fields of 5.6, 8.45 and 14.1 T. For the Si—O—Si resonance the dominance of the second-order quadrupolar interaction in determining the lineshape is clearly demonstrated with the linewidth (in ppm) narrowing closely with the inverse square of the applied field [10, 32, 33]. The Si—OH group resonates in this region and is a relatively sharp feature at ∼0 ppm that does not shift much with magnetic field [25]. At 5.6 T, in addition to the small spinning sidebands from the Si—O—Si resonance, there are clearly additional resonances at ∼250, 360, and 540 ppm. On increasing the magnetic field to 8.45 T

TABLE II Summary of ^{29}Si MAS NMR results and simulations for $(TiO_2)_x(SiO_2)_{1-x}$ samples with varying calcination temperature and composition

Sample (x, calcination temperature)	Q^2			Q^3			Q^4		
	δ (ppm) (±0.5)	Int. (% of total) (±2)	Width (ppm) (±0.5)	δ (ppm) (±0.5)	Int. (% of total) (±2)	Width (ppm) (±0.5)	δ (ppm) (±0.5)	Int. (% of total) (±2)	Width (ppm) (±0.5)
0.08, NHT	−93.9	12	8.8	−101.5	41	6.7	−108.7	48	9.8
0.08, 250°C	−92.9	11	10.2	−100.9	34	7.6	−109.6	56	9.2
0.08, 500°C	−93.6	5	10.0	−100.2	14	9.7	−109.3	82	13.0
0.08, 750°C	−94.0	3	3.0	−103.0	7	7.0	−111.3	90	10.5
0.18, NHT	−92.0	25	14.9	−101.1	27	6.1	−109.7	48	9.4
0.18 250°C	−93.6	12	10.8	−100.5	24	8.1	−108.0	65	12.0
0.18 500°C	−92.5	3	9.0	−99.8	14	9.0	−109.1	83	12.4
0.18 750°C	ND	ND	ND	−102.0	8	6.4	−112.0	92	11.8
0.41, NHT	−92.6	10	9.0	−101.3	31	7.4	−110.3	59	9.8
0.41, 250°C	−92.7	8	9.4	−101.3	33	7.4	−110.9	58	8.7
0.41, 500°C	−92.0	9	9	−102.0	33	9.0	−110.0	58	8.8
0.41, 750°C	−94.0	2	4.1	−100.5	10	7.4	−110.8	89.3	12.6

ND—Not detected.

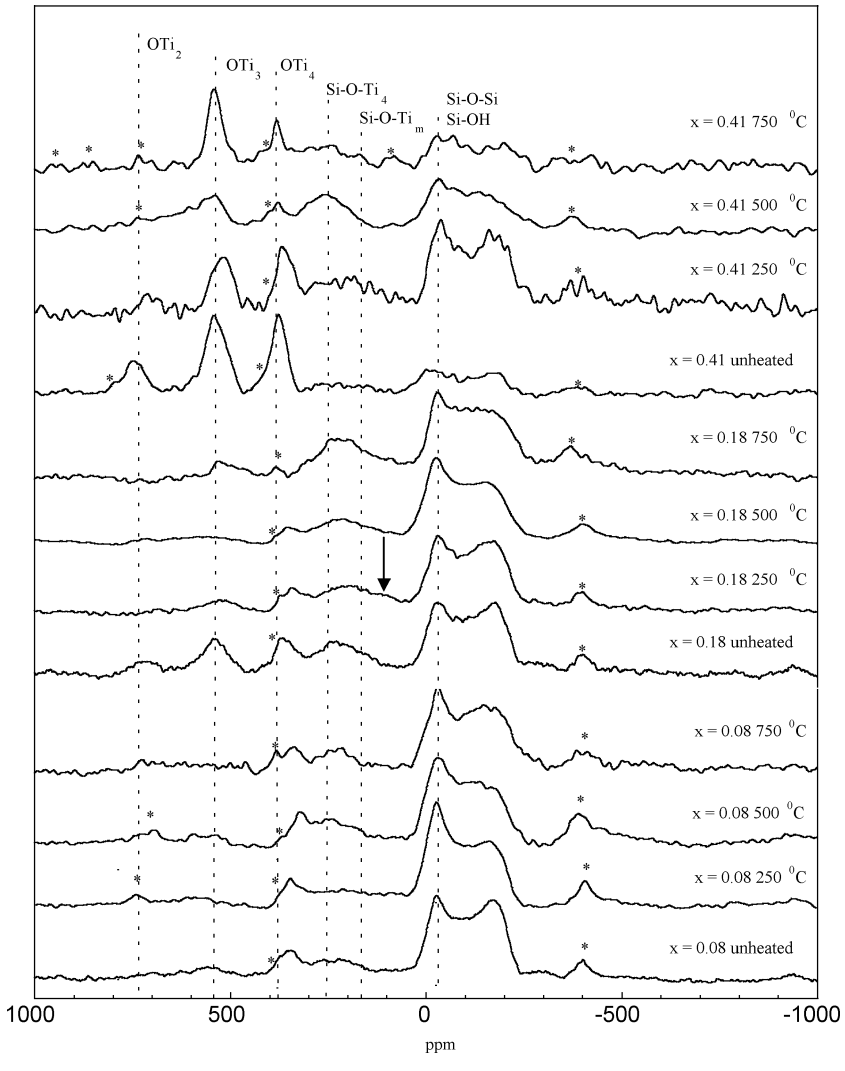

Figure 5 ^{17}O MAS NMR for $(TiO_2)_x(SiO_2)_{1-x}$ xerogels after various calcinations (* denote spinning sidebands).

these peaks are all very much reduced in amplitude, until by 14.1 T none of them are observed. The reason for the apparent absence of these resonances is a result of the relative changes of the dominant broadenings of the different resonances. For the lines at 360 and 540 ppm the chemical shift dispersion is dominant and the quadrupole interaction is negligible so that their linewidths scale directly with the applied magnetic field. At the highest fields the chemical shift dispersion width will be at its greatest. If the intrinsic width approaches the MAS rate then such sites will not narrow. Although any un-narrowed signal would be surprising at the MAS rates used here, there is some evidence in the 14.1 T data of broad underlying intensity (Fig. 6).

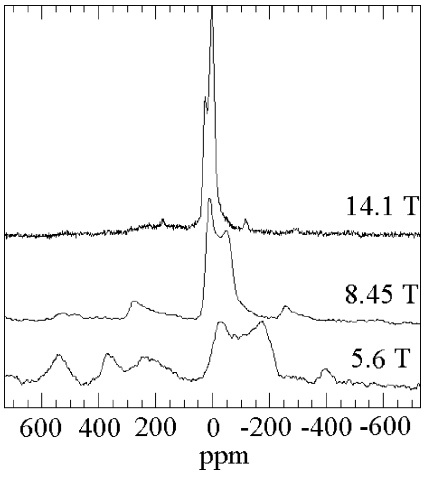

Figure 6 ^{17}O MAS NMR for unheated $(TiO_2)_{0.18}(SiO_2)_{0.82}$ as a function of applied magnetic field strength.

Additionally there is the cosmetic effect, that at the highest field, the narrowing of the quadrupole interaction means that the peaks whose width is dominated by it have much increased (relative) amplitudes. The peak at ∼250 ppm has a width which shows intermediate behaviour indicating that the two interactions are comparable for this peak. These observations are important in that they indicate that variable magnetic fields should be used to best understand the ^{17}O NMR spectra from such materials so that peaks indicating phase separation are not missed. Here it is lower applied magnetic field that is the most informative as the peaks where chemical shift dispersion is dominant are most easily seen at this field.

3.4. Diffraction experiments

The reciprocal space interference function or structure factor $S(Q)$ for some of the materials derived from X-ray diffraction is shown in Fig. 7 and the real space correlation function $T(r)$ curves in Fig. 8. An example fit to the experimental $T(r)$ data along with the individual correlations is shown in Fig. 9. The results of the fitting model $S(Q)$s are summarised in Table III.

The neutron-derived structure factors are presented in Fig. 10 and the $T(r)$ curves are shown in Fig. 11 for some of the materials. A fit (including the individual correlations) for the SiTi-8 sample heated to 750°C is also shown in Fig. 12 as an example. The results of fitting a model $S(Q)$ are given in Table IV.

4. Discussion

In our previous studies of unheated $(TiO_2)_x(SiO_2)_{1-x}$ xerogels, using XRD and ND [8], and EXAFS [34] on heated samples a number of observations about the structure were made. These included the SiTi-8 sample where titanium is four-fold coordinated in "silica-like" sites. For the SiTi-41 sample titanium is largely six-fold coordinate in "anatase-like" sites, implying phase separation (although there are still some four-fold sites present within the silicate phase). For the SiTi-18 sample the structure is more complex with both tetrahedral and octahedral titanium sites occurring in the unheated gels, but with the number of octahedral sites being reduced by heating. The importance of the SiTi-18 composition meant that a series of *in situ* studies combining EXAFS and XANES [35] and XRD [36] showed the initial gel is a mixture of TiO_4 and TiO_6 that becomes predominantly TiO_4 on heating, with this site showing very much reduced disorder. To check the mesoscopic heterogeneity SAXS experiments were carried out for the same samples [37]. SAXS showed that for the SiTi-41 sample phase separation was present at all temperatures, and it increased with heat treatment. There was no SAXS evidence for mesoscopic phase separation for the SiTi-8 and -18 samples at calcination temperatures

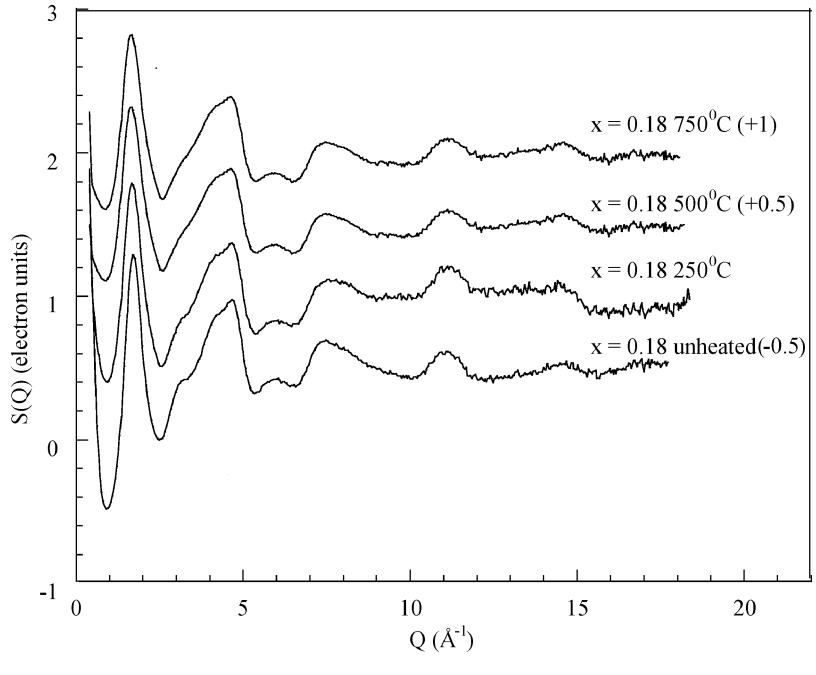

Figure 7 X-ray scattering data, $S(Q)$, for $(TiO_2)_{0.18}(SiO_2)_{0.82}$ samples after various calcinations (The data are offset for clarity).

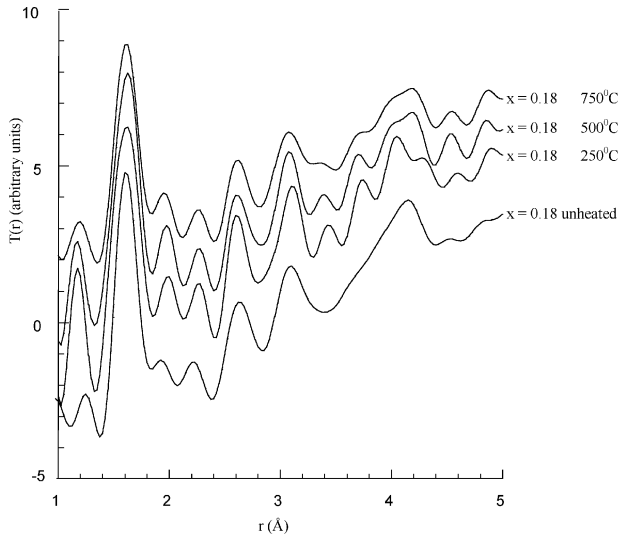

Figure 8 Correlation functions, $T(r)$, derived from the X-ray scattering data for the $(TiO_2)_{0.18}(SiO_2)_{0.82}$ sample after various calcinations (The data are offset for clarity).

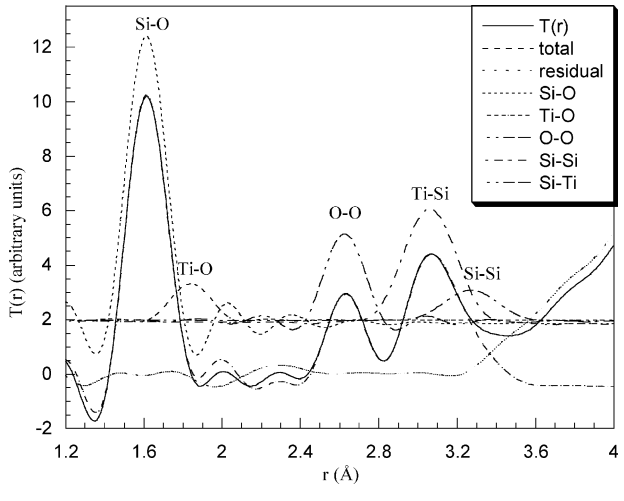

Figure 9 Example of a Gaussian simulation of the X-ray correlation function, $T(r)$, for $(TiO_2)_{0.08}(SiO_2)_{0.92}$ sample calcined at 500°C. (Note that the fitted peaks are offset for clarity).

below 750°C. For the SiTi-18 sample some phase separation could be seen after heating to 750°C.

The XANES approach of Farges *et al*. [38] was developed to identify the different titanium coordinations.

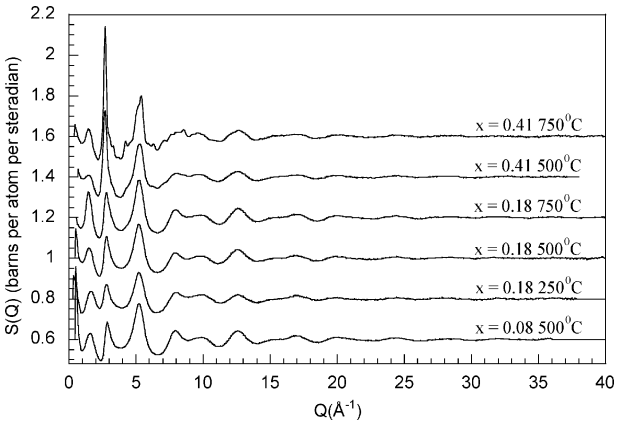

Figure 10 Neutron scattering data, $S(Q)$, for $x = 0.08$, 0.18, and 0.41 $(TiO_2)_x(SiO_2)_{1-x}$ samples after various calcinations. (Note that the Bragg peaks in the $x = 0.41$ sample can be assigned to crystalline TiO_2 in the form of anatase. The data are offset for clarity).

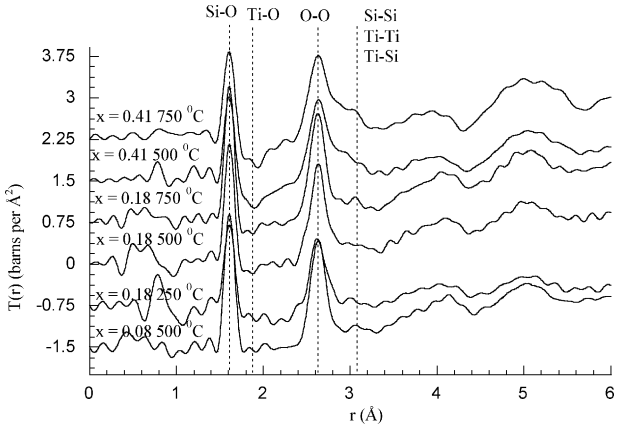

Figure 11 Correlation functions, $T(r)$, derived from the neutron scattering data for $x = 0.08$, 0.18 and 0.41 $(TiO_2)_x(SiO_2)_{1-x}$ samples after various calcinations. (Note that Ti—O and O—H correlations (at 1.8–1.92 and 0.95 Å respectively) are negative. (The data are offset for clarity).

In situ XANES [39] indicated that for the SiTi-8 and SiTi-18 samples the number of four-fold titanium sites in a gel previously unheated or calcined to 250°C increased markedly when heated for even just a few minutes and observed at temperature. When allowed to cool and left in ambient conditions for a short while, most of the newly formed four-fold sites reverted immediately back to six-fold. Interestingly, XANES indicates

TABLE III Summary of simulations of X-ray diffraction results for $(TiO_2)_x(SiO_2)_{1-x}$ samples with varying calcination temperature and composition

Sample	Si—O			Ti—O		
(x, calcination temp)	r (Å)	n_{ij}	σ (Å)	r (Å)	n_{ij}	σ (Å)
0.08, unheated	1.61 (±0.05)	3.4 (±1)	0.08 (±0.02)	–	–	–
0.08, 250°C	1.61 (0.05)	3.8 (±1)	0.08 (±0.02)	–	–	–
0.08, 500°C	1.61 (±0.01)	3.7 (±1)	0.06 (±0.02)	–	–	–
0.08, 750°C	1.61 (±0.05)	3.7 (±1)	0.08 (±0.02)	–	–	–
0.18, unheated	1.61 (±0.05)	3.4 (±0.5)	0.08 (±0.02)	–	–	–
0.18, 120°C	1.62 (±0.05)	4.2 (±0.5)	0.11 (±0.02)	–	–	–
0.18, 250°C	1.63 (±0.05)	4.3 (±0.5)	0.11 (±0.02)	–	–	–
0.18, 500°C	1.62 (±0.05)	3.8 (±0.5)	0.09 (±0.02)	–	–	–
0.18, 750°C	1.62 (±0.05)	4 (±1)	0.08 (±0.02)	–	–	–
0.41, unheated	1.57 (±0.05)	3.4 (±1)	0.07 (±0.02)	–	–	–
0.41, 250°C	1.60 (±0.01)	4 (±1)	0.07 (±0.02)	1.93 (±0.02)	6 (±1)	0.13 (±0.03)
0.41, 500°C	1.62 (±0.01)	3 (±1)	0.04 (±0.02)	1.92 (±0.02)	6 (±1)	0.10 (±0.03)

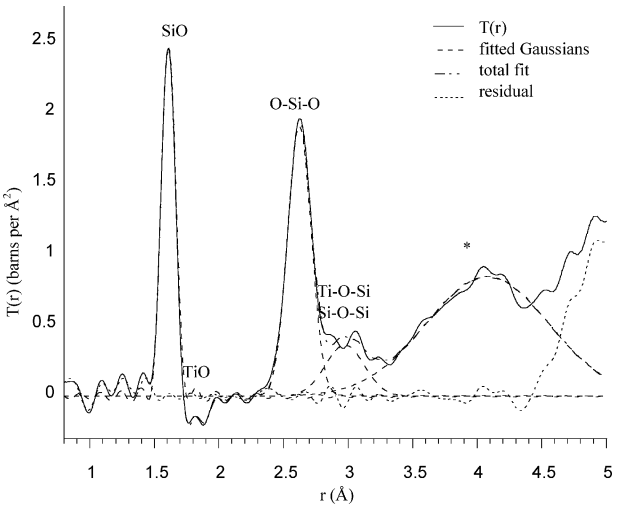

Figure 12 Example of a Gaussian simulation of the neutron correlation function, $T(r)$, for $(TiO_2)_{0.08}(SiO_2)_{0.18}$ calcined at 500°C.

some six-fold coordinated groups for the SiTi-8 sample, while there was no evidence for this from EXAFS. The implication is that these 4/6 fold reversible sites are probably structurally four-fold sites with two associated water molecules providing the extra oxygen atoms, which were beyond the detection limits of earlier experiments. Detailed XANES reveals the complexity of these amorphous TiO_2-SiO_2 materials [40] since there are four distinct titanium sites within the structure (depending on composition) that can be identified viz. (1) octahedral sites from phase separated TiO_2, (2) octahedral sites within the SiO_2 network, (3) octahedral sites that have coordinated water molecules that are rapidly converted to tetrahedral on heating and (4) tetrahedral sites within the SiO_2 framework. The presence of 4-fold coordinated titanium in SiTi-18 samples has been observed by a number of groups [41, 42] using EXAFS and XANES. Lui *et al*. [43] also report a mixture of four and six-fold coordinated sites in a SiTi-11 gel. Ti—O—Si linkages are also reported in FTIR studies [22, 44, 45].

A number of studies using ^{29}Si MAS NMR, with and without cross-polarisation have been reported [46–49]. ^{29}Si MAS NMR can provide somewhat ambiguous information about the nature of the cross-linking, and is most valuable when used in conjunction with other techniques. All of these studies are indicative of a progressive increase in cross-linking (i.e., an increasing proportion of Q^4) with increasing calcination temperatures. Early NMR studies suggested that the Q^2 and Q^3 signals detected were from SiO_4 units with titanium next nearest neighbours, and used this as evidence of titanium entering the network. However other studies, including the present one, show that in xerogels where Ti—O—Si bonds are known to exist, give ^{29}Si MAS NMR spectra that correspond mostly to Q^4. This implies that the Q^4 resonance must include all $Si(OSi)_x(OTi)_{1-x}$ ($0 \leq x \leq 4$, titanium in tetrahedral coordination). The Q^4 line width is consistent with this interpretation as it increases with heat treatment, corresponding to an increasing range of variation of next nearest neighbours. This is also supported by a recent theoretical study of the isotropic ^{29}Si chemical shift which showed that a change of ~1 ppm occurs per titanium second neighbour [50]. If Q^2 and Q^3 peaks do occur in calcined samples where other terminating groups (e.g., OH) are largely removed this must indicate that some titanium is acting as a network modifier. ^{17}O NMR however has seen limited use to date, despite the sensitivity of this technique to distinguish different sites in oxides. For $(TiO_2)_x(SiO_2)_{1-x}$ Delattre [26] reported ^{17}O NMR from sols prior to gelation.

The data collected here are entirely consistent with previous experimental work in the literature, but allows a much more detailed interpretation of the data when taken as a whole. The first observation is that the ^{29}Si MAS NMR spectra from the unheated xerogels indicates significant Q^2 and Q^3 contents (see Table II, and Fig. 4) that must correspond to OH and ethoxy groups attached to the central silicon. FTIR also indicates the presence of hydroxyl groups (see Fig. 3). As the material is calcined the number of terminating groups is reduced—increasing the cross-linking of the network until it is almost fully cross-linked after heating to 750°C. FTIR shows the progressive loss of hydroxyls and organic groups from the network as indicated by ^{1}H NMR [11], and ND shows the reduction in area of the hydrogen correlation (see Table IV and Fig. 11) with increasing calcination temperature. It should also be noted that for the SiTi-18 sample calcined to 250°C the hydrogen correlations (C—H and O—H) are centred at 1.06 Å, which implies both C—H (1.1 Å) and O—H (0.95–1.02 Å) [51] groups are present. After calcination to 500°C the hydrogen correlation occurs at ca. 0.96 Å, at all concentrations of Ti, indicating that the terminating groups are largely hydroxyls and that most organic groups have been eliminated. This agrees with a detailed ^{13}C MAS NMR study that shows that the residual organic fragments are lost around 250°C [11]. After calcination at 750°C no O—H correlation was detected for either SiTi-41 or -18 samples. This again agrees with our recent quantitative ^{1}H NMR work that shows that only signal consistent with surface, rather than structural hydroxyl remains at 750°C [11]. The ^{29}Si MAS NMR data indicated that after heating to 750°C the silicate part of the structure is almost completely cross-linked.

FTIR data of the SiTi-18 and SiTi-8 samples calcined at 850°C shows the presence of a very few OH groups. This suggests that all the xerogels initially contain a significant amount of hydroxyl and organic network terminating groups. On calcination the number of these terminating groups is reduced. At 500°C most of the organic groups have been removed from the network, and by 750°C the network has very nearly completely condensed, again agreeing with NMR.

Looking in detail at the SiTi-8 xerogel a number of points are apparent. The ^{17}O NMR spectra (Fig. 5) are dominated by the Si—O—Si signal at 0 ppm. In this sample after all heat treatments, a signal at ~235 ppm is observed which can be assigned to Ti—O—Si. A lot of work has been devoted to understanding oxygen resonances in this region including of model titanodiphenylsiloxanes that have TiO_2-SiO_2-like cores [27], $LiTiSiO_5$ [52] and $CaTiSiO_5$ [53]. There is some evidence that that Si—O—TiO_5 resonates at a more positive shift than

TABLE IV Summary of simulations of neutron diffraction results for $(TiO_2)_x(SiO_2)_{1-x}$ samples with varying calcination temperature and composition

Sample	O–H			Si–O			Ti–O			O–O (via Si)		
(x, calcination temp)	r (Å)	n_{ij}	σ (Å)	r (Å)	n_{ij}	σ (Å)	r (Å)	n_{ij}	σ (Å)	r (Å)	n_{ij}	σ (Å)
0.08, 500°C	0.96 (±0.02)	0.9 (±0.4)	0.04 (±0.005)	1.61 (±0.01)	4.0 (±0.2)	0.051 (±0.004)	1.86 (±0.01)	[a]	0.016 (±0.02)	2.63 (±0.01)	5.3 (±0.3)	0.089 (±0.008)
0.18, 250°C	1.06 (±0.02)	[a]	0.054 (±0.002)	1.61 (±0.01)	4.5 (±0.5)	0.052 (±0.002)	1.84 (±0.01)	7 (±3)	0.099 (±0.002)	–	–	–
0.18, 500°C	0.96 (±0.02)	1.0 (±0.2)	0.040 (±0.008)	1.61 (±0.01)	4.0 (±0.2)	0.052 (±0.005)	1.84 (±0.01)	3 (±1)	0.081 (±0.005)	2.62 (±0.01)	4.3 (±0.2)	0.081 (±0.006)
0.18, 750°C	–	–	–	1.61 (±0.01)	4.2 (±0.4)	0.052 (±0.001)	1.81 (±0.02)	4 (±1)	0.100 (±0.010)	2.62 (±0.01)	5.4 (±0.5)	0.091 (±0.001)
0.41, 500°C	–	–	–	1.61 (±0.01)	4.0 (±0.3)	0.052 (±0.001)	1.90 (±0.01)	5 (±1)	0.120 (±0.006)	2.62 (±0.01)	3.8 (±0.3)	0.090 (±0.003)
0.41, 750°C	–	–	–	1.61 (±0.01)	4.3 (±0.4)	0.055 (±0.001)	1.91 (±0.01)	6 (±1)	0.14 (±0.01)	–	–	–

[a] denotes that a meaningful coordination number was not obtained.

Si–O–TiO_3 [27] although the regions are very close, and it is still an open question as to whether the ^{17}O chemical shift can be used to unambiguously determine the titanium coordination. In Fig. 5 the different possible regions are marked. In the xerogel heated to 250°C this feature is notably weaker. Ti–O–Si linkages can also be seen in the FTIR data. ND data for the sample heated to 500°C (Table IV) indicates a bond length of 1.84 Å for the Ti–O correlation. Although the X-ray data (Table III) cannot resolve the Ti–O correlation, an asymmetry on the high r edge of the Si–O peak can be seen at all temperatures (Fig. 8). This indicates the presence of a Ti–O correlation at a similar distance to that of the neutron data. This is also in agreement with a previous EXAFS study [34] which indicates a bond length of around 1.84 Å. ^{29}Si MAS NMR shows that by 750°C the Q^4 species is dominant at ∼90%. This data taken together provides unequivocal evidence that the $x = 0.08$ sample has a silica-like structure, with the titanium atoms largely incorporated substitutionally in this structure.

The SiTi-41 sample has very different characteristics. Observation of the structure factors from both X-ray and neutron diffraction (Figs 7 and 10 respectively) show the appearance of Bragg peaks at ≥500°C attributed to crystalline anatase. The ^{17}O NMR spectra (Fig. 5) all show a strong signal at 530 ppm, characteristic of OTi_3 in an anatase-like environment [31], in addition to the 0 ppm Si–O–Si peak. The unheated gel also shows a very strong peak at 360 ppm and a smaller peak at 750 ppm; these may be attributed to OTi_4 and OTi_2 respectively [30]. The small and relatively broad peak between 110 and 300 ppm has been assigned to Ti–O–Si links, with a range of connected titanium sites present. On heating to 250°C OTi_2 is eliminated and a significant increase in Ti–O–Si signal is observed. The increase in intensity is most observable around ∼235 ppm. On heating to 500°C the Ti–O–Si peak at ∼235 ppm again increases in intensity, this time at the expense of OTi_3 and OTi_4. Interestingly this is the point at which crystallisation is first observed, which is also marked by the highest degree of atomic mixing. At 750°C the OTi_3 signal dominates the spectrum with OTi_4, and some Ti–O–Si and Si–O–Si. The broadness of the Si–O–Si resonance at this applied magnetic field results in its amplitude being quite low. ND for samples heated to 500 and 750°C (Fig. 11 and Table IV) both show a long Ti–O bond length (1.90 and 1.91 Å respectively) and coordination numbers of 5 ± 1 and 6 ± 1 This again is a clear indication that the titanium is primarily in octahedral sites, although the bond length is a slightly shorter than usually associated with Ti–O in octahedral units. However the width of the correlation in both cases is large ($\sigma \sim 0.12$ and 0.14 Å) and could easily encompass a minority proportion of tetrahedral titanium sites. XRD data (Fig. 8 and Table III) supports this conclusion. The unheated xerogel has a particularly wide Ti–O correlation, which can be attributed to the presence of the OTi_2 sites seen in the ^{17}O NMR. The diffraction data is in broad agreement with the previous EXAFS study [34]. Partial crystallisation of this material at 500°C and above, and the presence of octahedral titanium sites provides evidence that this material shows some phase separation. However the continued presence of Ti–O–Si cross-linking associated with tetrahedral units suggests that some titanium remains in the silicon-rich phase. The importance for the atomic scale structure of the preparation details is highlighted by comparing the structure obtained here with that when the titanium precursors reactivity is reduced by prior reaction with acetylacetone. When the reactivity is slowed during the initial stages significantly more Ti–O–Si linkages form for SiTi-41 samples, indicating improved mixing of the components in the initial gel and that these persist under heat treatment [22].

Initially the SiTi-18 sample shows some titanium clustering as ^{17}O MAS NMR (Fig. 5) shows the presence of OTi_3. There is also a strong Ti–O–Si signal at ∼235 ppm. The shoulder on the low ppm side suggests the presence of some Ti–O–Si linkages associated with different local configurations. On heating to 250°C the OTi_3 signal has largely disappeared, and a shoulder on the Ti–O–Si signal at ∼110 ppm is far more pronounced. This suggests that Ti–O–Ti linkages are being broken and converted to Ti–O–Si links. At 500°C the ∼110 ppm shoulder on the 250 ppm peak has become weaker, indicating an increase in the number of sites. On calcination at 750°C there is a further

reduction in the ~110 ppm shoulder, accompanied by the reappearance of a OTi_3 feature which can be seen as a peak at 530 ppm. *In situ* XANES [39] gave similar results, showing an increase in tetrahedral sites up to 750°C but with the tetrahedral:octahedral ratio never reaching a maximum value as observed for the SiTi-8 sample. FTIR spectroscopy shows the presence of Ti—O—Si linkages at all temperatures. The neutron diffraction data (see Table IV, Fig. 11) shows the Ti—O correlation to be at a distance of 1.82–1.84 Å and a coordination number of 4 indicative of tetrahedral coordination. The X-ray $T(r)$s do not have sufficient resolution to allow reliable fitting of the Ti—O correlation, however its presence can be seen as a shoulder (1.84 Å) on the Si—O peak at 1.62 Å. From the ^{29}Si MAS NMR data most of the titanium has to be tetrahedrally coordinated in these samples. The presence of some $Q^{2,3}$ means that there must be a small amount of higher coordination titanium present acting as a network modifier.

On calcination to 750°C the SiTi-18 sample begins to show some genuine phase separation. This coincides with the point at which no terminating groups remain. Previous XANES [40] and SAXS [37] studies indicated that calcination at 1000°C causes a reduction in the number of tetrahedral sites, and a small amount of phase separation. In melt quenched titania-silica glasses phase separation occurs when the titanium concentration is sufficient to produce a significant number of Ti—O—Ti links when randomly distributed into network silicon sites [41, 42, 54]. When the SiTi-18 xerogel network is complete at 750°C (e.g., when its structure becomes close to that of a conventional glass) it begins to phase separate. Before this point, although some titanium *may* occur in clusters, as the silica-based network is not yet fully formed (i.e., not all Q^4), combined with the high degree of Ti—O—Si cross-linking, phase separation is discouraged.

In both the neutron data and in the previous EXAFS study [34], the Ti—O bond length for SiTi-8 and SiTi-18 xerogels is longer (1.84 Å) at calcination temperatures of up to 500°C than it is after calcination at 750°C (1.82 Å). Since the SiTi-8 xerogels do not contain octahedral titanium sites, this contraction cannot be attributed to the removal of structural octahedral titanium sites. However, reversible 4/6 fold titanium sites associated with OH termination are present after calcination at temperatures up to 500°C but are much reduced or completely removed after calcination at 750°C. Since the EXAFS and diffraction experiments were carried out in ambient conditions, the longer Ti—O bond length may be attributed to the presence of reversible 4/6 fold titanium sites which are six-fold coordinate at the time of measurement.

Thus it is possible to produce a model of the structure that is consistent with interpretation of all of the NMR, diffraction, EXAFS, XANES, SAXS and IR data, which would have been highly speculative if based on a smaller subset of these techniques. The characterisation methodology used here provides an extremely detailed picture of the structure of these complex amorphous materials and will aid understanding of their structural development and the foundation of their technological properties. Such information is already being used to correlate structural features with properties such as catalytic activity [e.g., 55, 56].

5. Conclusions

All these $(TiO_2)_x(SiO_2)_{1-x}$ xerogels initially contain a significant number of hydroxyl and organic groups which terminate the silicate network after formation. On calcination to successively higher temperatures the organic and hydroxyl contents are reduced, and cross-linking of the silicate network increases. After calcination at 500°C the organic groups have all been removed. Calcination at 750°C removes almost all of the hydroxyl groups and the silicate network is highly condensed (e.g., average $Q^{3.9}$). The SiTi-8 xerogel has a silica-like structure in which titanium is mostly substituted into silicon sites. The SiTi-41 xerogel is phase separated and anatase crystallises at 500°C. There is still some atomic mixing, however, with titanium substitution in the silicon-rich phase. The SiTi-18 xerogel exhibits more complex behaviour. Although initially there is some clustering of the titanium, revealed by Ti—O—Ti linkages, a very high level of atomic mixing exists. On calcination at moderate temperatures (≤500°C) this atomic mixing increases further. However this structure is unstable to calcination at higher temperatures (750°C and above) and phase separation begins to occur although again a substantial amount of the titanium remains in the silicate phase.

Acknowledgements

EPSRC are thanked for funding this work through several grants, especially GR/L28647, GR/N64151 and GR/N64267, and the funding of NMR spectrometers at Warwick through JREI awards, and for funding PhD studentships (RA, GWW and PG).

References

1. C. J. BRINKER and G. W. SCHERER, "Sol-Gel Science, The Physics and Chemistry of Sol-Gel Processing" (Academic Press, San Diego, 1990).
2. J. B. MILLER, S. T. JOHNSTON and E. I. KO, *J. Catal.* **150** (1994) 311.
3. D. R. UHLMANN, T. SURATWALA, K. DAVIDSON, J. M. BOULTON and G. TEOWEE, *J. Non-Cryst. Solids* **218** (1997) 113.
4. G. BRUSATIN, M. GUGLIELMI, P. INNOCENZI, A. MARTUCCI, G. BATTALJLIN, S. PELLI and G. RIGHINI, *ibid.* **220** (1997) 202.
5. R. J. DAVIS and Z. LUI, *Chem. Mater.* **9** (1997) 2311.
6. B. E. YOLDAS, *J. Non-Cryst. Solids* **38**/**39** (1980) 81.
7. P. J. DIRKEN, M. E. SMITH and H. J. WHITFIELD, *J. Phys. Chem.* **99** (1995) 395.
8. J. S. RIGDEN, J. K. WALTERS, P.J. DIRKEN, M. E. SMITH, G. BUSHNELL-WYE, W. S. HOWELLS and R. J. NEWPORT, *J. Phys: Condens. Matter* **9** (1997) 4001.
9. G. ENGELHARDT and D. MICHEL, "High Resolution Solid State NMR of Silicates and Zeolites" (John Wiley and Sons, Chichester, 1987).
10. K. J. D. MACKENZIE and M. E. SMITH, "Multinuclear Solid State NMR of Inorganic Materials" (Pergamon Press, Oxford, 2002).

11. P. N. GUNAWIDJAJA, M. A. HOLLAND, G. MOUNTJOY, D. M. PICKUP, R. J. NEWPORT and M. E. SMITH, *Solid State NMR*, **23** (2003) 88.
12. B. E. WARREN, "X-ray Diffraction" (Addison-Wesley Publishing Company, Reading Massachusetts, USA, 1969).
13. D. T. CROMER and J. B. MANN, *Acta Cryst.* A **24** (1968) 321.
14. F. HADJU, *ibid.* **27** (1971) 73.
15. "International Tables For Crystallography, Vol. C, Mathematical Physical and Chemical Tables," edited by A. C. J. Wilson (Kluwer Academic Publishers, Dordrecht, Germany).
16. J. Z. TURNER, A. K. SOPER, W. S. HOWELLS, A .C HANNON and S. ANSELL, "SANDALS Survival Guide Version 2.2" ISIS Facility Rutherford Appleton Laboratory, Didcot Oxford, UK (unpublished).
17. A. K. SOPER, W. S. HOWELLS and A. C. HANNON, "ATLAS Analysis Of Time Of Flight Data From Liquid and Amorphous Samples," ISIS Facility Rutherford Appleton Laboratory, Didcot, Oxford (1997) (unpublished).
18. A. C. HANNON, W. S. HOWELLS and A. K. SOPER, *IOP Conference Series* **107** (1990) 193.
19. J. F. BENT, "An Experimental Study Of Some Silicate Based Glasse," Ph.D. Thesis, University of Warwick, UK, 1999.
20. P. H. GASKELL in "Materials Science and Technology: Glasses and Amorphous Materials," Vol. 9, edited by J. Zrzycky (Weinham, VCH, 1991).
21. G. ORCEL, J. PHALIPPOU and L. L. HENCH, *J. Non-Cryst. Solids* **88** (1986) 114.
22. D. M. PICKUP, G. MOUNTJOY, G. W. WALLIDGE, R. ANDERSON, J. M. COLE, R. J. NEWPORT and M. E. SMITH, *J. Mater. Chem.* **9** (1999) 1299.
23. A. LABOURIAU, T. J. HIGLEY and W. L. EARL, *J. Phys. Chem.* B **102** (1998) 2897.
24. T. H. WALTER, G. L. TURNER and E. OLDFIELD, *J. Magn. Reson.* **76** (1988) 106.
25. E. R. H. VAN ECK, M. E. SMITH and S. C. KOHN, *Solid State NMR* **15** (1999) 181.
26. L. DELATTRE and F. BABONNEAU, *Chem. Mater.* **9** (1997) 2385.
27. C. GERVAIS, F. BABONNEAU, D. HOEBBEL and M. E. SMITH, *Solid State NMR* **17** (2000) 2.
28. C. GERVAIS, F. BABONNEAU and M. E. SMITH, *J. Phys. Chem.* B **105** (2001) 1971.
29. J. BLANCHARD, C. BONHOMME, J. MACQUET and C. SANCHEZ, *J. Mater. Chem.* **8** (1998) 985.
30. E. SCOLAN, C. MAGNENET, D. MASSIOT and C. SANCHEZ, *ibid.* **9** (1999) 2467.
31. T. J. BASTOW, A. F. MOODIE, M. E. SMITH and H. J. WHITFIELD, *ibid.* **3** (1993) 697.
32. M. E. SMITH and E. R. H. VAN ECK, *Prog. Nucl. Magn. Reson. Spectr.* **34** (1999) 159.
33. A. P. M. KENTGENS, *Geoderma* **80** (1997) 271.
34. R. ANDERSON, G. MOUNTJOY, M. E. SMITH and R. J. NEWPORT, *J. Non-Cryst. Solids* **232–234** (1998) 72.
35. D. M. PICKUP, G. MOUNTJOY, M. A. HOLLAND, G. W. WALLIDGE, R. J. NEWPORT and M. E. SMITH, *J. Phys.: Condens. Matter* **12** (2000) 9751.
36. D. M. PICKUP, G. MOUNTJOY, M. A. ROBERTS, G. W. WALLIDGE, R. J. NEWPORT and M. E. SMITH, *ibid.* **12** (2000) 3521.
37. G. MOUNTJOY, J. S. RIGDEN, R. ANDERSON, G. W. WALLIDGE, R. J. NEWPORT and M. E. SMITH, *J. Mater. Res.* **15** (2000) 1998.
38. F. FARGES, G. E. BROWN and J. J. REHR, *Phys. Rev.* B **56** (1997) 1807.
39. G. MOUNTJOY, D. M. PICKUP, G. W. WALLIDGE, J. M. COLE, R. J. NEWPORT and M. E. SMITH, *Chem. Phys. Lett.* **304** (1999) 150.
40. G. MOUNTJOY, D. M. PICKUP, G. W. WALLIDGE, R. ANDERSON, J. M. COLE, R. J. NEWPORT and M. E. SMITH, *Chem. Mater.* **11** (1999) 1253.
41. D. R. SANDSTROM, F. W. LYTLE, P. S. P. WEI, R. B. GREEGOR, J. WONG and P. SCHULTZ, *J. Non-Cryst. Solids* **41** (1980) 201.
42. R. B. GREEGOR, F. W. LYTLE, D. R. SANDSTROM, J. WONG and P. SCHULTZ, *ibid.* **55** (1983) 27.
43. Z. LUI and R. J. DAVIS, *J. Phys.Chem.* **98** (1994) 1253.
44. I. M. MIRANDA SALVADOR and J. M. FERDINANDEZ NAVARRO, *J. Non-Cryst. Solids* **147/148** (1992) 256.
45. M. SCHRAML-MARTH, K. L. WALTHER, A. WOKAUN, B. E. HANDY and A. BAIKER, *ibid.* **143** (1992) 93.
46. K. L. WALTHER, A. WOKAUN, B. E. HANDY and A. BAIKER, *ibid.* **134** (1991) 47.
47. J. MENDEZ-VIVAR, R. MENDOZAR-SERNA, J. GOMEZ-LARA and G. GAVINO, *J. Sol-Gel Sci. Tech.* **8** (1997) 235.
48. J. M. MIILER and L. J. LAKSHMI, *J. Phys. Chem.* B **102** (1998) 6465.
49. Z. LUI, G. M. CRUMBAUGH and R. J. DAVIS, *J. Catal.* **159** (1996) 83.
50. G. RICCHIARDI and J. SAUER, *Z. Phys. Chem.* **209** (1999) 21.
51. "CRC Handbook Of Chemistry and Physics," 62nd ed, edited by R. C. Weast and M. J. Astle (CRC Press, Boca Raton, Florida, 1982).
52. T. J. BASTOW, G. A. BOTTON, J. ETHERIDGE, M. E. SMITH and H. J. WHITFIELD, *Acta Cryst.* A **55** (1999) 127.
53. S. KROEKER, D. RICE and J. F. STEBBINS, *Amer. Mineral.* **87** (2002) 572.
54. D. L. EVANS, *J. Non-Cryst. Solids* **52** (1982) 115.
55. M. A. HOLLAND, D. M. PICKUP, G. MOUNTJOY, E. S. C. TSANG, G. W. WALLIDGE, R. J. NEWPORT and M. E. SMITH, *J. Mater. Chem.* **10** (2000) 2495.
56. C. BECK, T. MALLAT, T. BURGI and A. BAIKER, *J. Catal.* **204** (2001) 428.

Received 3 March 2003
and accepted 20 January 2004